Optics Letters

87-W 1018-nm Yb-fiber ultrafast seeding source for cryogenic Yb: yttrium lithium fluoride amplifier

Yi Hua,[1] Wei Liu,[1] Michael Hemmer,[1] Luis E. Zapata,[1] Gengji Zhou,[1] Damian N. Schimpf,[1,2] Tino Eidam,[3,4] Jens Limpert,[3,4] Andreas Tünnermann,[3,4] Franz X. Kärtner,[1,2,5] and Guoqing Chang[1,2,*]

[1]Center for Free-Electron Laser Science, DESY, Notkestraße 85, 22607 Hamburg, Germany
[2]The Hamburg Centre for Ultrafast Imaging, Luruper Chaussee 149, 22761 Hamburg, Germany
[3]Institute of Applied Physics, Abbe Center of Photonics, Friedrich-Schiller-Universität Jena, Albert-Einstein-Strasse 15, 07745 Jena, Germany
[4]Helmholtz Institut Jena, Fröbelstieg 3, 07743 Jena, Germany
[5]Physics Department, University of Hamburg, Luruper Chaussee 149, 22761 Hamburg, Germany
*Corresponding author: guoqing.chang@desy.de

Received 17 January 2018; revised 8 March 2018; accepted 8 March 2018; posted 12 March 2018 (Doc. ID 319283); published 6 April 2018

We demonstrate a compact and robust Yb-fiber master-oscillator power-amplifier system operating at 1018 nm with 2.5-nm bandwidth and 1-ns stretched pulse duration. It produces 87-W average power and 4.9-μJ pulse energy, constituting a powerful seed source for cryogenically cooled ultrafast Yb: yttrium lithium fluoride (Yb:YLF) amplifiers.

OCIS codes: (140.3490) Lasers, distributed-feedback; (140.3280) Laser amplifiers; (140.7090) Ultrafast lasers.

https://doi.org/10.1364/OL.43.001686

High-energy pulses at high average power with subpicosecond (sub-ps) duration at 1 μm wavelength are desired in many applications, such as soft x-ray generation [1], optical parametric chirped pulse amplifier pumping [2], terahertz radiation generation and amplification, as well as high-brightness photoinjectors for laser Wakefield acceleration or free-electron lasers [3]. Room temperature Yb: yttrium aluminum garnet (Yb:YAG) laser systems are becoming commonplace for producing high average power and high energy sub-ps optical pulses due to their high electrical-to-optical efficiency and broadband emission spectrum. Cryogenically cooling Yb:YAG in composite thin-disk geometries can further scale up the average power at the expense of a reduced emission bandwidth that cannot deliver sub-ps pulses [4]. In contrast, cryogenically cooled Yb: yttrium lithium fluoride (Yb:YLF) has a gain bandwidth of several nanometers centered at 1018 nm, enough to support sub-ps pulse operation [5,6]. Together with a high saturation fluence, a longer excited state lifetime, and a smaller quantum defect than Yb:YAG, cryogenically cooled Yb:YLF has the potential for realizing sub-ps laser sources featuring both high pulse energy and high average power. The larger gain bandwidth of cryogenically cooled Yb:YLF is also advantageous for the application of the chirped-pulse amplification (CPA) technique. However, a seed laser operating at 1018 nm central wavelength and with a large stretching factor is required to permit efficient and damage-free energy extraction in the subsequent 100 mJ-class amplifiers under construction [7]. In a previous implementation of a cryogenic Yb:YLF CPA laser system, a Ti:sapphire laser was used as the seeder to reach 100 W at 10 kHz [6]. However, the low seeding pulse energy (~1 nJ) at wavelength of 1018 nm required numerous passes in subsequent amplifiers with unfavorable consequences on stability and spectral narrowing due to the large gain required to achieve 10 mJ level pulse energy.

A high-energy (μJ to sub-mJ) seeding source will facilitate the implementation of a 100 mJ cryogenically cooled Yb:YLF amplifier chain by mitigating amplified spontaneous emission (ASE) and gain-narrowing in the onwards amplifier chain. Such μJ-to-mJ pulse energy can be achieved in an ultrafast Yb-fiber amplifier system employing large-mode-area double cladding gain fiber or rod-type gain fiber [8,9]. However, all of these high energy sub-ps sources operate at ~1030 nm. Indeed, Yb-fiber exhibits a broad gain bandwidth, allowing laser operation in the wavelength range between 976 and 1120 nm [10]. To date, the reported high-power Yb-fiber lasers at around 1018 nm produce either continuous waves [11,12] or pulses of several picoseconds in duration [13]. Sub-ps high power sources at 1018 nm specially designed for seeding cryogenic cooling YLF have never been reported before. Apart from the lack of a seed source with sub-ps transform-limited pulse duration, amplifying 1018 nm in an Yb-doped fiber front end is another challenge because Yb-fiber lasers operate as three-level systems for the signal wavelength below 1030 nm [14]. Consequently, the relatively small emission cross section and high absorption cross section require high inversion pumping and short gain fiber length to prevent signal reabsorption that decreases the slope efficiency of the Yb-fiber amplifier system. Additionally the ASE around 1030 nm competes with the signal at 1018 nm for up-level population. To suppress the ASE at 1030 nm and efficiently amplify signal at 1018 nm, high inversion pumping or specialty gain fibers are necessary. During the amplification, spectral broadening and wavelength shifting should be also carefully controlled.

In this Letter, we demonstrate the first high-power fiber-based system specifically designed to seed a high energy

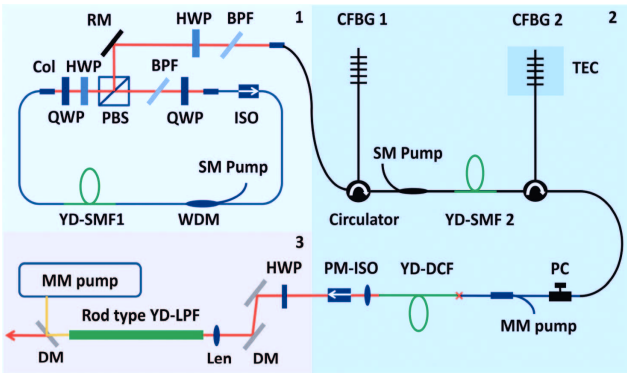

Fig. 1. Schematic of 1018-nm MOPA system including three parts: Yb-fiber oscillator (Part 1), two stages of pulse stretcher and preamplifier (Part 2), and rod-type Yb-fiber power amplifier (Part 3). HWP, half-wave plate; QWP, quarter-wave plate; BPF, bandpass filter; PBS, polarization beamsplitter; RM, reflecting mirror; Col, collimator; WDM, wavelength division multiplexer; SM, single mode; MM, multimode; CFBG, chirped fiber Bragg grating; PC, polarization controller; PM-ISO, polarization sensitive isolator; DM, dichroic mirror; YD, ytterbium-doped; SMF, single mode fiber; DCF, double-clad fiber; LPF, large-pitch fiber. Non-PM fiber, PM fiber, and Yb-doped fiber are denoted by the blue line, black line, and green line, respectively.

Yb:YLF amplifier chain. With a repetition rate of 17.88 MHz, the fiber-based master-oscillator power amplifier (MOPA) front end employs the CPA technique and produces 87-W, 4.9-μJ pulses centered at 1018 nm with 1-ns stretched duration. The amplification is achieved by two stages of specially designed fiber amplifiers that suppress the ASE at 1030 nm.

Figure 1 shows the experimental setup consisting of three parts: an Yb-fiber oscillator, two stages of fiber stretchers with preamplifiers, and a rod-type power amplifier. Part 1 is a 17.88-MHz all-normal-dispersion (ANDi) oscillator at 1020 nm mode-locked by nonlinear polarization evolution in combination with an intracavity bandpass filter (BPF) [15]. The BPF has 4-nm transmission bandwidth, and the center wavelength can be tuned by tilting its incident angle. The passive fiber is 10 and 0.5 m long before and after the 0.4-m gain fiber (Coractive Yb 501), respectively. This ANDi laser relies on the narrow bandpass filter for wavelength selection and energy dissipation to achieve stable mode-locking at the target wavelength. The shortest and longest center wavelength achieved by the ANDi laser is usually limited by the pump power, the cavity length, and the emission spectrum of the gain fiber inside the cavity [16]. The longest wavelength ever reported for ANDi mode-locked fiber lasers is 1070 nm [17], while the shortest is 1024 nm [16]. Further blueshifting the center wavelength is extremely challenging because low gain and large gain dispersion may prevent mode-locking.

We first carry out numerical simulation to investigate the mode-locking of this Yb-fiber oscillator at ~1018 nm. The intracavity pulse built up is modeled by the generalized nonlinear Schrödinger equation incorporating a simplified saturable absorber model, in which the transmittance of the effective saturable absorber is given by $T = 1 - l_0/[1 + P(t)/P_{sat}]$. l_0 is the unsaturated loss, $P(t)$ the instantaneous pulse power, and P_{sat} the saturation power [18]. The Yb-fiber gain has a Lorenz line shape centered at 1030 nm with 40-nm bandwidth.

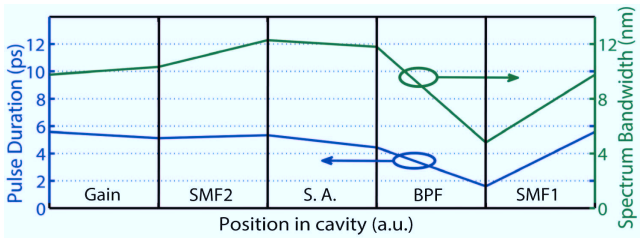

Fig. 2. Simulation of spectral bandwidth (green curve, full width at tenth of the maximum) and pulse duration (blue curve, full width at half of the maximum) inside the oscillator cavity. GAIN, 0.4-m high doping Yb-fiber; SMF2, 0.5-m single mode fiber; SA, saturated absorber; BPF, narrow bandpass filter at 1020 nm with 4-nm bandwidth; SMF1, 10-m single mode fiber.

A 4-nm bandwidth filter (super-Gaussian shape) with a tunable central wavelength selects the target mode-locking wavelength in the cavity. By shifting the central wavelength of the filter to 1020 nm, the oscillator reaches a stable mode-locking state. The evolution of pulse duration and spectral bandwidth inside the cavity is shown in Fig. 2, revealing the features of similariton evolution as a result of the narrow bandpass filter and large passive fiber length [15]. Both the pulse duration and the spectral bandwidth breathe during a round trip.

Figures 3(a)–3(c) present the simulation results on the spectral and temporal properties of the Yb-fiber oscillator. The laser output spectrum [blue curve in Fig. 3(a)] centers at 1020 nm with 10-nm bandwidth and covers the key spectral component around 1018 nm. Further tuning the spectrum to shorter wavelengths leads to failure of mode-locking because the increased wavelength mismatch with the Yb-fiber peak gain reduces the round-trip gain to a value that cannot compensate for the intracavity loss. Figure 3(b) shows the temporal profile of the output pulse (blue curve) with positive chirp (green curve). The asymmetric pulse shape is due to the gain dispersion, which destroys

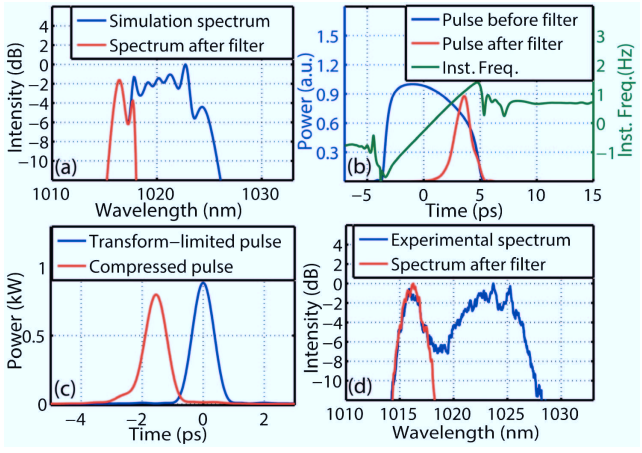

Fig. 3. (a) Simulation of oscillator output spectrum (blue curve) and spectrum after filter (red curve) with 2.5 nm bandwidth at 1016. (b) Simulation of output pulse (blue curve) with nonlinear chirp (green curve) and filtered pulse (red curve). (c) Simulation of transform-limited pulse (blue curve) and compressed pulse (red curve) after spectral filtering. (d) Measured output spectrum of oscillator (blue curve); spectrum after BPF with 2 nm bandwidth at 1016 nm (red curve) in experiment. Inst. Freq., instantaneous frequency.

the symmetry of the similariton pulse and its linear chirp [19]. Another super-Gaussian bandpass filter placed outside the cavity selects a 2.5-nm-wide spectral band centered at 1016 nm [red curve in Fig. 3(a)]. We intentionally pick the wavelength slightly shorter than 1018 nm such that it shifts to longer wavelength in the subsequent fiber components due to nonlinear propagation. The corresponding filtered pulse is shown as the red curve in Fig. 3(b). Although the whole output pulse exhibits strong nonlinear chirp, the pulse given by the filtered spectrum is located at the tail of the overall pulse and is almost linearly chirped. Numerical compression of the pulse after filtering by a pair of transmission gratings (groove density: 1000 lines/mm) is compared with the transform-limited pulse in Fig. 3(c), demonstrating the feasibility of good pulse compression.

Guided by the simulations, we construct the Yb-fiber oscillator. The blue curve in Fig. 3(d) shows the experimentally achieved broadband oscillator output, which covers 1015–1025 nm with a 2-nm spectral lobe centered at 1016 nm. A comparison between Figs. 3(a) and 3(d) shows that the numerical simulation agrees qualitatively with the experimental results. We use a bandpass filter to select the spectral lobe at 1016 nm [red curve in Fig. 3(d)] and then free-space couple it into the subsequent polarization maintaining (PM) fiber that belongs to Part 2 of our setup.

Part 2 includes two PM fiber-pigtailed circulators connected to two PM chirped fiber Bragg gratings (CFBGs) with 7.5-nm reflection bandwidth centered at 1019 nm. These CFBGs are designed to compensate for the dispersion of a 1760 lines/mm grating-pair compressor operated at 60-deg incidence angle. The first CFBG has a chirp rate of −306 ps/nm and the second one −100 ps/nm. Considering that the nonlinear length is about 0.2 m for a 1-nJ transform-limited Gaussian pulse with 2-nm spectrum bandwidth, we expect that the spectrum of the input pulse broadens in the passive fiber prior to the first CFBG. Relying on both this spectral broadening and the CFBG filtering, the target wavelength around 1018 nm can be readily achieved. This is confirmed by the simulation in which we numerically propagate a 1-nJ, 800-fs transform-limited Gaussian pulse (corresponding to 2-nm bandwidth) in 0.8 m of passive fiber. As Fig. 4(a) shows, the initial Gaussian spectrum (red curve) evolves into two spectral lobes mainly due to self-phase modulation. The spectral lobe on the longer side peaks at ∼1018 nm and is selected by the CFBGs. The simulation results are confirmed by the measured output spectrum from Part 2 [blue curve in Fig. 4(b)] that is redshifted compared with the input spectrum [red curve in Fig. 4(b)]. During the experiment, we adjust the passive fiber length and fine tuning the input pulse energy to achieve the output spectrum with 2.5 nm bandwidth centered at 1018 nm. The bandwidth is 0.5 nm larger than the emission spectrum of cryogenic YLF (2 nm), which precompensates for the gain narrowing in the cryogenic Yb:YLF amplifier. The two stages of CFBGs stretch the pulse to ∼1 ns duration [Fig. 4(c), measured using a 20-GHz bandwidth photodiode attached to a 4-GHz bandwidth oscilloscope], therefore alleviating nonlinear effects in subsequent amplifier stages. A preamplifier based on a 3-m-long, low doping gain fiber (Nufern PM-YSF-LO) is inserted between the two circulators to compensate the losses introduced by the circulators and CFBGs. There is no noticeable

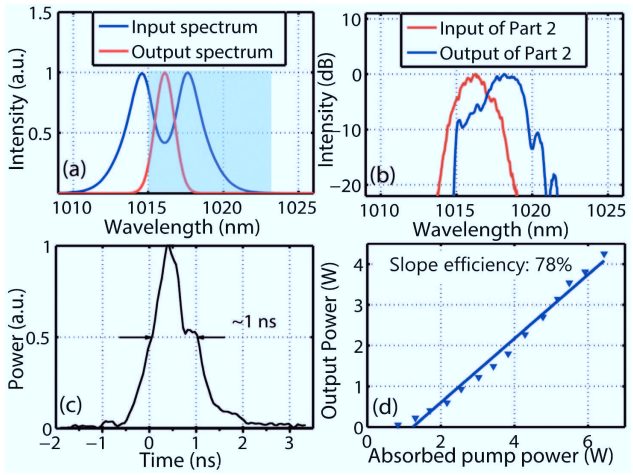

Fig. 4. (a) Simulation of 800-fs, 1-nJ transform-limited Gaussian pulse propagating through 0.8-m passive fiber. Red curve: input spectru;, blue curve: output spectrum; blue shadow: reflection bandwidth of the CFBG. (b) Measured spectra at the input (red curve) and output (blue curve) of Part 2. (c) Measured pulse after two stages of CFBGs. (d) Measured output power versus absorbed pump power in the flattened absorption Yb-fiber amplifier.

wavelength shifting in this amplifier stage owing to the high level of inversion in the gain fiber [20].

The second amplifier that is spliced directly to port 3 of circulator 2 is constructed from 1-m flattened absorption Yb-doped double-clad fiber (Coractive DCF-YB-8/128P-FA). Usually, Yb-doped fiber lasers exploit the quasi-four-level system between 1030 and 1100 nm [21]. For wavelength below 1030 nm, Yb-fiber operates as a three-level system, making amplification of sub-ps pulses at 1018 nm difficult due to the low emission cross section and high absorption cross section at shorter wavelength. Fortunately, the flattened absorption Yb-fiber is specially designed to suppress ASE at 1030 nm and provides higher gain at 1018 nm than 1030 nm [12]. As a result, the Yb-fiber amplifier efficiently amplifies the signal wavelength to 4-W average power with a very high slope efficiency of 78% at a wavelength of 1018 nm [Fig. 4(d)] and negligible ASE. Although the Yb-fiber is non-PM, adjusting the polarization controller at the combiner input results in 18-dB polarization extinction ratio.

The maximum output from Part 2 is 4 W, corresponding to 223-nJ pulse energy. This energy level is sufficient for seeding a 10-mJ class cryogenically cooled YLF amplifier and subsequent 100-mJ class amplifiers. Indeed, more power extracted from the fiber front end leads to less gain needed for the following 100-mJ-level cryogenic YLF amplifiers. Since the cryogenically cooled gain crystal has a relatively narrow gain spectrum of only 2 nm compared with Yb-doped fiber amplifiers with 40 nm bandwidth, increasing the seed power directly from the fiber can mitigate the gain narrowing effect in subsequent amplifier stages and, therefore, allows obtaining sub-ps duration pulses in the final amplifier stage [22]. Because the pulse is stretched to ∼1 ns, further amplification to higher pulse energy levels can be readily achieved. To demonstrate this possibility, Part 3 is constructed, which is a power amplifier using a 1.2-m long Yb-doped, rod-type large pitch fiber (LPF) for further energy

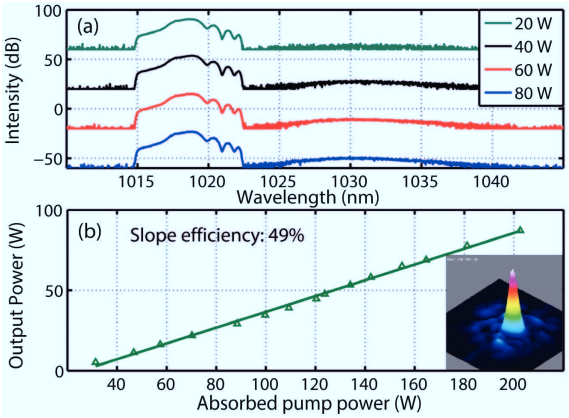

Fig. 5. (a) Output power versus absorbed pump power of rod-type LPF amplifier and spatial profile (inset). (b) Output spectra of rod-type LPF amplifier at 1018 nm for increasing pump powers.

boosting [23]. The special design of large core diameter (80 μm) and robust single mode operation allows for high energy extraction with diffraction-limited beam quality. It is noteworthy that the unique double cladding structure of rod-type LPF with the small clad-to-core area ratio is critical for achieving a relatively high slope efficiency to amplify wavelengths shorter than 1030 nm with negligible ASE [14,24].

Figure 5(a) shows the output spectra versus average power of the amplified pulses. The signal spectra remain unchanged, suggesting a linear amplification. Broadband ASE peaking at 1030 nm grows with the increased pump power, yet remains 26 dB below the signal spectral peak even at the highest average power of 87 W. The slope efficiency of the LPF amplifier is 49% [Fig. 5(b)], which is higher than was achieved from other rod-type LPF laser systems working at the same wavelength around 1018 nm [10].The inset of Fig. 5(b) shows the excellent spatial profile of the 87-W amplified pulses, corresponding to a pulse energy of 4.9 uJ. Due to the limited input signal power level of the rod-type fiber amplifier, we restrict the final power output to below 100 W in order to avoid the onset of harmful parasitic oscillation at the ASE peak.

In conclusion, we report a high-power 17.88 MHz Yb-fiber MOPA system operating at 1018 nm with 87-W average power. The ASE at 1030 nm is efficiently suppressed during amplification using specially designed flattened absorption fiber and rod-type LPF. It is the first powerful fiber front end designed especially for a 100 mJ, sub-ps duration cryogenic Yb:YLF amplifier chain with its output spectrum precisely matching the gain of Yb:YLF crystals, and the bandwidth is slightly larger to compensate for the gain narrowing effect. The 4.9-μJ pulse energy is the highest pulse energy at 1018 nm achieved by fiber laser systems. We are planning to further increase the pulse energy by reducing the pulse repetition rate. At 1-ns stretched pulse duration, linear amplification to mJ pulse energy is feasible [9]. Since the main scope of this work is to develop a suitable front-end seeding source for a cryogenic Yb:YLF amplifier chain, we leave the amplified pulses uncompressed. Indeed, they can be compressed using a pair of transmission gratings (groove density: 1700 lines/mm). We recently implemented a 1018-nm front end with the similar design and seeded a 100-mJ-level cryo Yb:YLF amplifier chain. The amplified pulses were compressed to 1.2 ps while the transform-limited duration is 800 fs. Such a deviation can be mitigated by incorporating a temperature gradient to fine-tune the dispersion property of the CFBG stretcher.

Funding. Helmholtz-Gemeinschaft through Helmholtz Young Investigator (VH-NG-804); Deutsches Elektronen Synchrotron, H2020 European Research Council (ERC) (609920); The Hamburg Centre for Ultrafast Imaging—Structure, Dynamics and Control of Matter at the Atomic Scale of the Deutsche Forschungsgemeinschaft (DFG) (EXC 1074).

REFERENCES

1. F. Krausz and M. Ivanov, Rev. Mod. Phys. **81**, 163 (2009).
2. S. Witte and K. S. E. Eikema, IEEE J. Sel. Top. Quantum Electron. **18**, 296 (2012).
3. C. Hernandez-Garcia, M. L. Stutzman, and P. G. O'shea, Phys. Today **61**(2), 44 (2008).
4. L. E. Zapata, F. Reichert, M. Hemmer, and F. X. Kärtner, Opt. Lett. **41**, 492 (2016).
5. L. E. Zapata, Proc. SPIE **7686**, 768607 (2010).
6. D. E. Miller, L. E. Zapata, D. J. Ripin, and T. Y. Fan, Opt. Lett. **37**, 2700 (2012).
7. M. Hemmer, L. E. Zapata, Y. Hua, and F. X. Kaertner, *Advanced Solid-State Photonics* (Optical Society of America, 2016), paper ATh4A.3.
8. J. S. Feehan, J. H. V. Price, T. J. Butcher, W. S. Brocklesby, J. G. Frey, and D. J. Richardson, Appl. Phys. B **123**, 43 (2017).
9. M. Kienel, M. Müller, A. Klenke, J. Limpert, and A. Tünnermann, Opt. Lett. **41**, 3343 (2016).
10. R. Royon, J. Lhermite, L. Sarger, and E. Cormier, Opt. Express **21**, 13818 (2013).
11. C. Ottenhues, T. Theeg, K. Hausmann, M. Wysmolek, H. Sayinc, J. Neumann, and D. Kracht, Opt. Lett. **40**, 4851 (2015).
12. J. Wang, G. Chen, L. Zhang, J. Hu, J. Li, B. He, J. Chen, X. Gu, J. Zhou, and Y. Feng, Appl. Opt. **51**, 7130 (2012).
13. X. Qi, S. P. Chen, H. Y. Sun, B. Yang, and J. Hou, Opt. Express **24**, 16874 (2016).
14. J. Boullet, Y. Zaouter, R. Desmarchelier, M. Cazaux, F. Salin, J. Saby, R. Bello-Doua, and E. Cormier, Opt. Express **16**, 17891 (2008).
15. W. H. Renninger, A. Chong, and F. W. Wise, IEEE J. Sel. Top. Quantum Electron. **18**, 389 (2012).
16. X. Xiao, Y. Hua, B. Fu, and C. Yang, IEEE Photon. J. **5**, 1502807 (2013).
17. L. Kong, X. Xiao, and C. Yang, Laser Phys. **20**, 834 (2010).
18. F. Ö. Ilday, J. R. Buckley, W. G. Clark, and F. W. Wise, Phys. Rev. Lett. **92**, 213902 (2004).
19. D. B. Soh, J. Nilsson, and A. B. Grudinin, J. Opt. Soc. Am. B **23**, 10 (2006).
20. R. Paschotta, J. Nilsson, A. C. Tropper, and D. C. Hanna, IEEE J. Quantum Electron. **33**, 1049 (1997).
21. A. Silva, K. J. Boller, and I. D. Lindsay, Opt. Express **19**, 10511 (2011).
22. P. Raybaut, F. Balembois, F. Druon, and P. Georges, IEEE J. Quantum Electron. **41**, 415 (2005).
23. J. Limpert, F. Stutzki, F. Jansen, H. J. Otto, T. Eidam, C. Jauregui, and A. Tünnermann, Light Sci. Appl. **1**, e8 (2012).
24. F. Beier, H. J. Otto, C. Jauregui, O. de Vries, T. Schreiber, J. Limpert, R. Eberhardt, and A. Tünnermann, Opt. Lett. **39**, 3725 (2014).